SAND2021-4026C

ILASS-Americas 31st Annual Conference on Liquid Atomization and Spray Systems, May 2021

Similarity In Non-Evaporating, Mixing-Limited Sprays

David P. Schmidt*[1] and Marco Arienti[2]

[1]Department of Mechanical and Industrial Engineering, University of Massachusetts, Amherst, MA 01003 USA
[2]Thermal/Fluid Sciences and Engineering, Sandia National Laboratories, Livermore, CA 94550 USA

Abstract

Starting with a well-tested, one-dimensional model of non-evaporating, mixing-limited sprays, the governing equations for liquid mass and two-phase momentum can be manipulated to reveal the formal similarity between momentum and liquid volume fraction. These quantities are integrated over a cross-section of the spray, including the presence of a radial profile. The consequence of this mathematical observation is that momentum, when properly non-dimensionalized, is equal to the liquid volume fraction at any time and at any axial location within a non-evaporating, mixing-limited spray with a constant rate of injection. We compare the predictions of this mathematical analysis to high-fidelity, first-principles simulation results of a non-evaporating spray to assess the validity of the assumed similarity. The mathematical derivation shows that momentum and liquid volume fraction are essentially the same quantity in non-evaporating, mixing-limited sprays. The analysis of the simulation confirms this result, but also points to the difference between the radial profile of velocity and the radial profile of LVF (or density). This discrepancy indicates the need to re-examine the simplification that Musculus and Kattke made in modeling the momentum flux in view of the high density ratio that typically exist between liquid and gas.

*Corresponding Author: schmidt@acad.umass.edu

Introduction

The statistician George Box coined the phrase that "All models are wrong, but some are useful." One of the more useful models of transient, non-evaporating sprays was developed by Musculus and Kattke [1] based on the principle of mixing-limited spray evolution [2]. This model includes the ability to capture transient effects and radial profiles in liquid volume fraction (LVF) and velocity. The validity of the model was checked against experimental data by subsequent publications such as Musculus [3], Pickett et al. [4], Kook and Pickett [5], and Bardi et al. [6]. Often, the model is employed by fitting spray angle or coefficient of area of the nozzle, but the wide applicability and excellent agreement is still noteworthy.

This paper mathematically manipulates the governing equations of this model and reveals that the liquid volume fraction and spray momentum are formally similar. This means that the two quantities are equal. The present analysis builds upon the proposal by Musculus [3] that "the jet fluid is transported equally with velocity, so that the local mixture fraction can be represented by the local axial velocity relative to the original nozzle exit velocity." The present analysis reaches a slightly different conclusion, where the local mixture fraction instead depends on the ratio of momentum, rather than velocity.

Analogously, the present analysis independently addresses the assertion of Kastengren et al. [7] who proposed that the liquid mass, integrated in a slice transverse to the source of injection, should be proportional to mass-averaged velocity of the liquid. Like Musculus [3], the end result of Kastengren's analysis is a proportionality between velocity and liquid mass. In contrast, the present work will derive a relationship where the ambient gas density is a factor in the proportionality. Also, the analysis of Kastengren et al. applies only to portions of the spray that have achieved steady-state while the present work will derive a result that applies to the entire spray.

The equivalence of liquid volume fraction and momentum offers an opportunity for extracting additional information from experimental studies. The consequence of this discovery is that an experiment need only experimentally measure one of the two quantities in order to reveal the other. The result also offers some basic insights into spray physics in a succinct mathematical form.

Review of the Musculus-Kattke model

Our analysis begins with the governing equations used by Musculus and Kattke. The complete description is given in their paper [1] but a summary will be given here. The model employs a one-dimensional finite volume approach with a radial profile of velocity and mixture fraction, as illustrated in Fig. 1.

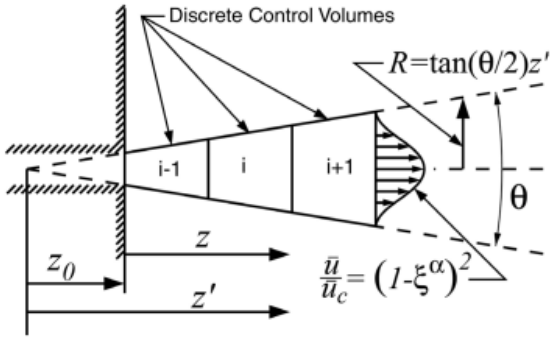

Figure 1. The Eulerian control volumes used in the Musculus-Kattke model. Taken from Musculus-Kattke(2009)

The authors then make a series of assumptions, summarized in the following list.

1. Non-evaporating spray
2. Constant densities of both liquid and gas phases
3. Turbulent stresses are neglected
4. Axial mixing is neglected
5. Axial pressure gradients are neglected
6. Spray angle is constant
7. The normalized radial profile of velocity remains constant after the end of injection

These assumptions then give rise to the basic conservation of mass and momentum equations for each control volume. The conservation of liquid fuel mass, m_f is given in Eqn. 1 and the equation for linear momentum flux, M, is given in Eqn. 2. Note that the momentum flux is for both phases, although the mass conservation equation is only for the liquid phase.

$$\frac{\partial m_f}{\partial t} = \dot{m}_{f,in} - \dot{m}_{f,out} \tag{1}$$

$$\frac{\partial M}{\partial t} = \dot{M}_{in} - \dot{M}_{out} \tag{2}$$

The liquid mass flux is defined using an integral across the cross-section of the jet. Note that both phases are assumed to move at the same velocity, $\bar{u}$, and the velocity is Reynolds-averaged. Here, ρ_f is the liquid density and dA is the differential cross-sectional area of the jet. The quantity $\bar{X_f}$ is the liquid volume fraction. The overbar on X_f signifies a cross-sectionally averaged quantity.

$$\dot{m}_f = \rho_f \int X_f u dA \tag{3}$$

Similarly, the momentum flux is also defined using an integral. However, since the momentum is for both phases, a mixture density is required that represents a weighted average of the two phase densities. In contrast, the overbar on u signifies a cross-sectionally averaged quantity, like $\bar{X_f}$.

$$\dot{M} = \int \bar{\rho} u^2 dA \tag{4}$$

Because the mixture density varies with location, it must remain within the integral of Eqn. 4. The mixture density is a simple function of the liquid volume fraction $\bar{X_f}$.

$$\bar{\rho} = \rho_f \bar{X_f} + \rho_a \left(1 - \bar{X_f}\right) \tag{5}$$

The evaluation of the integrals in Eqns. 3 and 4 is explained in detail by Musculus and Kattke. For the present work, it is sufficient to know that the integral results in the appearance of a parameter, β, that describes the shape of the jet profile. The β parameter is a measure of correlation between the X_f and u profiles, as shown in Eqn. 6.

$$\beta = \frac{1}{\bar{X_f}\bar{u}} \int X_f u dA \tag{6}$$

For a uniform radial profile, β is unity. For a fully developed profile, β is approximately 2. Though β represents a correlation between the two variables, X_f and u, the momentum flux depends on the square of velocity, requiring an assessment of X_f and u^2. However, Musculus and Kattke, for reasons of mathematical convenience, chose to use β in both calculation of mass and momentum flux. Thus, Eqns. 3 and 4 become:

$$\dot{m}_f = \beta \rho_f \bar{X_f} \bar{u} A \tag{7}$$

$$\dot{M} = \beta \bar{\rho} \bar{u}^2 A \tag{8}$$

These expressions are then applied by Musculus and Kattke to derive finite volume expressions for Eqns. 1 and 2. Each control volume has an axial extent Δz and a transverse area A. The liquid mass and total momentum for a control volume are then as follows.

$$m_f = \bar{X_f} \rho_f A \Delta z \tag{9}$$

$$M = \bar{\rho} \bar{u} A \Delta z \tag{10}$$

Finally, the partial differential equations Eqns. 1 and 2 are discretized to give expressions to update liquid mass and both phases' momentum in each control volume. The results are given in Eqns. 11 and 12.

$$m_{f,i}^{t+1} = m_{f,i}^t + \rho_f \left[\left(\beta \bar{X_f} \bar{u} A\right)_{i-1}^t - \left(\beta \bar{X_f} \bar{u} A\right)_i^t \right] \Delta t \tag{11}$$

$$M_i^{t+1} = M_i^t + \left[\left(\beta \bar{\rho} \bar{u}^2 A\right)_{i-1}^t - \left(\beta \bar{\rho} \bar{u}^2 A\right)_i^t \right] \Delta t \tag{12}$$

Analysis

The preceding section reviewed the equations of Musculus and Kattke. In this section, transport equations for liquid volume fraction and non-dimensional momentum are derived. The analysis will show that the transport equations for these two equations are identical and that the boundary conditions are identical. Because the solution for liquid volume fraction must be unique, the end result is that dimensionless momentum equals liquid volume fraction at any time and axial location in the spray.

The analysis begins with Eqns. 11 and 12, but could just as well start with the continuous equations 1 and 2. The first step is to recast the transport of liquid mass into liquid mass fraction. This process begins by dividing the equation by $\rho_f A \Delta z \Delta t$.

$$\frac{m_{f,i}^{t+1} - m_{f,i}^t}{\rho_f A \Delta z \Delta t} = \frac{\left[\left(\beta \bar{X_f} \bar{u} A\right)_{i-1}^t - \left(\beta \bar{X_f} \bar{u} A\right)_i^t \right]}{A \Delta z} \tag{13}$$

Note that ρ_f is a constant and $A\Delta z$ represents the finite volume. We use the definition of liquid volume fraction to replace m_f with $\bar{X_f}$.

$$\bar{X_f} = \frac{m_f}{\rho_f A \Delta z} \tag{14}$$

Inserting this expression in Eqn. 13 and taking the limits as both Δz and Δt approach zero gives us a partial differential equation for the transport of $\bar{X_f}$.

$$\frac{\partial \bar{X_f}}{\partial t} = \frac{-1}{A} \frac{\partial}{\partial z} \left(\beta \bar{X_f} \bar{u} A\right) \tag{15}$$

The result in Eqn. 15 is sufficient for the present purposes, but for clarity of interpretation, the equation can be rearranged in a Lagrangian form. First, apply the product rule to the expression on the right.

$$\frac{\partial \bar{X}_f}{\partial t} = -\beta\bar{u}\frac{\partial \bar{X}_f}{\partial z} - \frac{\bar{X}_f}{A}\frac{\partial}{\partial z}\left(\beta\bar{u}A\right) \tag{16}$$

Then, define a Lagrangian total derivative operator where the advection speed is defined as $\beta\bar{u}$. This advection speed shows that one consequence of the radial profile is to increase the advection speed.

$$\frac{D()}{Dt} \equiv \frac{\partial()}{\partial t} + \beta\bar{u}\frac{\partial()}{\partial z} \tag{17}$$

This operator can then be used to put Eqn. 16 into a Lagrangian form.

$$\frac{D\bar{X}_f}{Dt} = -\frac{\bar{X}_f}{A}\frac{\partial}{\partial z}\left(\beta\bar{u}A\right) \tag{18}$$

An examination of this equation shows that it is linear. Thus, for a given $\beta(z)$, $\bar{u}(z)$, and $A(z)$ there exists only one solution for $\bar{X}_f$. Also, the boundary conditions are unity at the injector orifice and zero in the limit of infinite z.

The next step is to perform an analogous manipulation of the momentum equation. This process begins by dividing the momentum equation, Eqn. 12 by $A\Delta z\Delta t$.

$$\frac{M_i^{t+1} - M_i^t}{A\Delta z\Delta t} = \frac{1}{A}\frac{\left[\left(\beta\bar{\rho}\bar{u}^2A\right)_{i-1}^t - \left(\beta\bar{\rho}\bar{u}^2A\right)_i^t\right]}{\Delta z} \tag{19}$$

Noting that A and Δz are not functions of time, the left side can be transformed into an expression for the time rate of change of $\bar{\rho}\bar{u}$. Using Eqn. 10 and taking the limits as Δt and Δz go to zero gives a partial differential equation for the transport of $\bar{\rho}\bar{u}$.

$$\frac{\partial \bar{\rho}\bar{u}}{\partial t} = \frac{-1}{A}\frac{\partial}{\partial z}\left(\beta\bar{\rho}\bar{u}^2A\right) \tag{20}$$

At this point, it is convenient to define a dimensionless linear momentum, L^*. The liquid density and injection velocity are used as reference scales. For steady injection conditions, the denominator is a constant and may be pulled into the temporal derivative. Whereas the density in the numerator is an average of the two phases, as defined by Eqn. 5, the density in the denominator represents only the liquid density.

$$L^* \equiv \frac{\bar{\rho}\bar{u}}{\rho_l u_{inj}} \tag{21}$$

Inserting this expression into equation 20 gives a result that is analogous to the transport of mass, Eqn. 15.

$$\frac{\partial L^*}{\partial t} = \frac{-1}{A}\frac{\partial}{\partial z}\left(\beta L^*\bar{u}A\right) \tag{22}$$

Applying the product rule and employing the same definition of Lagrangian derivative given in Eqn. 17, produces an expression for the evolution of momentum in the Lagrangian reference frame.

$$\frac{DL^*}{Dt} = -\frac{L^*}{A}\frac{\partial}{\partial z}\left(\beta\bar{u}A\right) \tag{23}$$

Comparing Eqn. 23 and 18 reveals the formal similarity. Except for the symbol $\bar{X}_f$ or L^*, these equations are identical. As for $\bar{X}_f$, the boundary condition for L^* is unity at the injector and zero in the far field. Hence, these are the same equations and the same boundary conditions. We then apply the idea of mathematical similarity: if these are the same equations and boundary conditions, then they have the same solution. The only remaining question is, are the solutions unique?

For non-linear partial differential equations, one must consider the possibility of multiple solutions. However, it will be assumed here that the solution for momentum transport is, like LVF, unique. Thus, the ultimate result of this derivation, Eqn. 24.

$$\boxed{\bar{X}_f = L^*} \tag{24}$$

The consequences of this result are that the liquid volume fraction and momentum ratio are the same at all times and axial locations in non-evaporating, mixing-limited sprays. Measuring one of these quantities provides knowledge of the other.

For example, if liquid volume fraction or velocity were available at a variety of transverse locations, one could use the fundamental definition of a cross-sectional average to calculate $\bar{X}_f$ or $\bar{u}$.

$$\bar{X}_f = \frac{1}{A}\int X_f dA \tag{25}$$

$$\bar{u} = \frac{1}{A}\int u dA \tag{26}$$

Though the value of u is strictly an average of the two phase velocities, the mixing-limited hypothesis assumes that the two phases are moving at the same velocity. Hence, if only liquid velocity data are available, these may be sufficient. The value of $\bar{\rho}$, required in the definition of L^*, can be calculated from $\bar{X}_f$ using Eqn. 5.

At a glance, the result of this paper may appear to be equivalent to that of Kastengren et al. [7] or

Musculus [3]. The difference is that the definition of momentum in the present work uses a density that is a weighted average of the gas and liquid density. Another subtle point of the present analysis is that if momentum and liquid volume fractions have the same transverse profile, then this result means at every location, LVF and momentum ratio are equal, without any transverse integration. The present result applies to any part of the spray.

However, one implication is contradictory to the initial assumptions: how can the momentum profile be similar to the LVF profile if LVF was assumed to have the same radial profile as velocity? This apparent mathematical contradiction is perhaps a consequence of the use of β in Eqn. 8, following Musculus and Kattke. Based on math and without regard for the resulting equation complexity, the momentum flux should include a parameter that represents a triple correlation.

Verification and Validation

The first step in showing the validity of this analysis is to test the predictions against the predictions of the Musculus-Kattke model from which the present results are derived. This test serves as a check of the mathematical analysis.

The prediction of Eqn. 24 is assessed in Fig. 2 for a high ambient pressure condition at an arbitrary time using a uniform rate of injection. The conditions are listed in Table 1. This figure shows both L^* and $\bar{X_f}$ plotted versus distance from the orifice using a line and symbols, respectively. No discrepancy between the two quantities is evident which indicates that indeed, dimensionless momentum is equal to LVF in the Musculus-Kattke model. The next step is to determine if this model corresponds to realistic sprays.

Parameter	**Value**
Gas density	33 $[kg/m^3]$
Fuel density	744 $[kg/m^3]$
Nozzle diameter	0.1 $[mm]$
C_a	1.0 $[-]$
Spray angle	21 $[degrees]$
Δz	0.05 $[mm]$
Inj. velocity	348 $[m/s]$

Table 1. Parameters used in the verification with the Musculus-Kattke model.

Validation of the analysis was conducted using the CLSVOF method applied to Spray D, as described in [8] and applied in [9]. While ideally, validation would involve experimental results, we have not been able to find such data in the open literature. The experimental data would require both liquid volume and velocimetry measurements from the same regions of the spray without recourse to assumptions such as Kastengren et al [7].

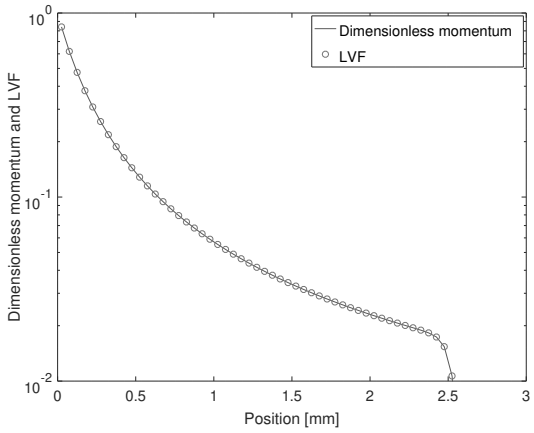

Figure 2. Verification with Musculus-Kattke model results. The dimensionless momentum and liquid volume fraction are plotted versus distance from the injector at a time of 0.01 ms after start of injection. The leading edge of the spray is at 2.5 mm

Spray D is a single axial hole injector which, in this case, was discharged into high pressure, low temperature nitrogen. The conditions are summarized in Table. 2, and the CFD code is described in a previous publication [10]. Figure 3 shows a snapshot of such simulation, including the resolved liquid surface and the cross-sectional planes that will be discussed in this Section. The simulation is designed to resolve (via interface reconstruction) the model-free dynamics of the liquid surface in a Direct Numerical Simulation (DNS) sense. As such, its analysis should be based on sample averaging of multiple DNS instances at a given time. This very expensive set of computations is avoided here by replacing sample averaging with time averaging, at the price of restricting the scope of the validation to the steady-state portion of the jet.

Parameter	**Value**
Liquid	n-Dodecane
Nozzle diameter	0.180 $[mm]$
Injection Pressure	150 $[MPa]$
Fuel Temperature	298 $[K]$
Gas density	22.8 $[kg/m^3]$
Ambient Temperature	298 $[K]$

Table 2. Parameters used in the CLSVOF Spray D simulation.

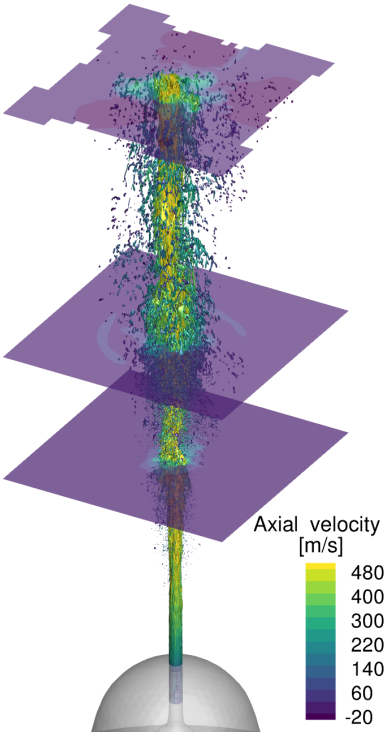

Figure 3. Snapshot of CLSVOF spray D simulation showing the resolved liquid surface and the cross-sectional planes used for analysis, all colored by axial velocity. The simulation includes the flow internal to the injector, which is partially visible in the picture.

Because the analysis in the current paper relies on a single, uniform nozzle velocity u_{inj}, we must extract this value from the CFD results. Conceptually, our goal is to represent the full exit profile with a reduced model as shown in Fig. 4. To do so, we follow the analysis of Payri et al. [11]. In this model, the value of u_{inj} is presumed to be equal to an effective velocity u_{eff} issuing over an areas A_{eff} that is less than the nozzle exit area. The values of u_{eff} and A_{eff} are calculated such that the effective area and velocity transit the same mass flow rate and momentum flux as the actual profile.

To calculate u_{eff} from the CFD results, we use the following algorithm. The value of u_{eff} is then used in place of u_{inj} in the above analysis.

1. Calculate the Bernoulli velocity, u_{th}, from the upstream and downstream pressures
2. Calculate the average velocity, $\bar{u}$ based on mass flow rate from the nozzle
3. Calculate the coefficient of discharge from $\bar{u}$

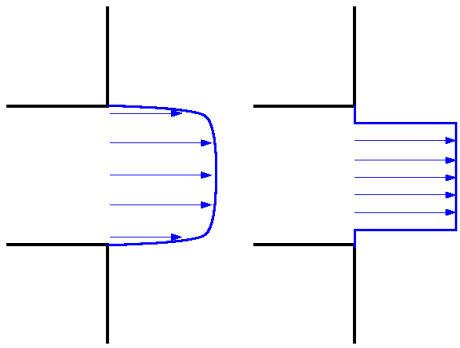

Figure 4. A sketch of the exit velocity profile and the modeling assumptions used in the current paper. The three-dimensional exit profile (left) must be represented as a uniform profile with equal mass and momentum flux (right).

4. Calculate the value of the momentum coefficient C_M from the ratio of momentum flux and $2A\Delta P$
5. $C_v = C_M/C_d$
6. The value of u_{eff} is $C_v u_{th}$

Next, the cross-sectionally averaged values of X_f and $\bar{u}$ are calculated from Eqns. 25 and 26. The application of the integral begs the question of the extent of the cross-sectional area. The velocity profiles from the CFD are wider than the LVF profiles, and so the results do show sensitivity to the spray angle, assumed to be 5.2 degrees in the present work. This discrepancy between the width of the LVF and velocity profiles are explored in the next section.

The results of the comparison are shown in Figures 5 and 6. The former figure shows the results on a linear scale as a function of distance downstream of the orifice. The latter figure tests the assertion that either momentum or velocity is equal to LVF. In neither case do the computations results convincingly confirm or refute the similarity. However, both views of the data show that momentum is more similar to LVF than velocity for this assumed value of spray angle.

An Examination of the Discrepancies

Axial velocity and LVF distribution are more closely examined in Figs. 7 and 8 at three jet cross-sections located at 7.8, 19, and 52 orifice diameters d_0 from the nozzle exit. The first position is selected to probe into the jet core region, which in the plots corresponds to the constant unit value of normalized axial velocity and LVF. Conversely, the 52 d_0 cross-section is taken almost at the end of the com-

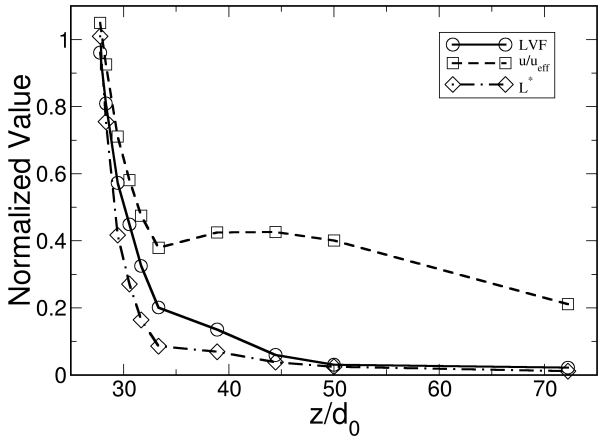

Figure 5. LVF, momentum ratio, and velocity ratio as a function of axial distance normalized by orifice diameter.

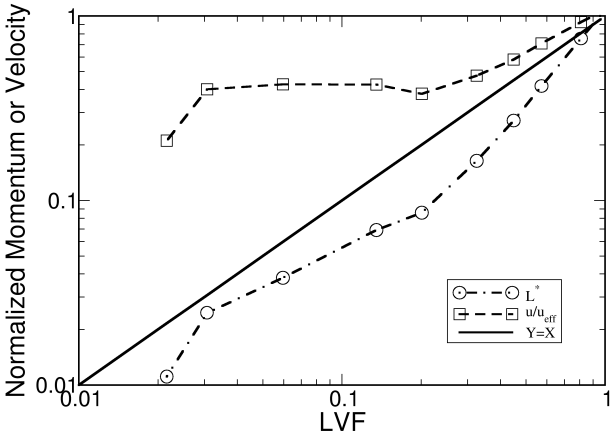

Figure 6. A comparison of the dependence of both L^* and normalized velocity u/u_{eff} on LVF. The third curve, $Y = X$ represents the theoretical equality of the two variables.

putational domain, where the liquid mass seems to approach a uniform distribution. In that position, the spray cone appears to be hollow, a feature that can reasonably be attributed to oscillations of the jet with respect to its geometrical axis on a longer period than the averaging window used here.

From a comparison of the two figures, it is apparent that each averaged LVF radial profile is substantially noisier than the corresponding axial velocity profile, a fact that can be explained in terms of surface tension coefficient opposing diffusion. Most of the features that are observed in the radial plots can therefore be expected to smooth out if the time average is extended for a sufficiently long period. More importantly, while the radial profiles show the same tendency to spread downstream of injection, this occurs at a much greater rate for velocity than for LVF because of the inertia of the liquid mass compared to the gas mass. This feature is visible in pictures of the spray simulations, such as the one displayed in Figure 3, where the gas region entrained by the jet is much broader than the spray cone at every cross-sectional plane. It is noted that the most downstream cross-section shows a relatively uniform velocity profile, with 40% decrease compared to the maximum value, in a region with radius of at least $2d_0$. Because of the large density ratio between liquid and gas, we can deduce that the normalized momentum of the flow and the liquid volume fraction of the jet eventually tend to follow a very similar radial profile, as concluded by our mathematical derivation.

Conclusions

A mathematical derivation has shown that momentum and liquid volume fraction are essentially the same quantity in non-evaporating, mixing-limited sprays, according to a one-dimensional model. This result, similar to a unity Schmidt number [1] assumption, indicates the analogous transport of liquid mass and momentum. Aside from the basic physical insight that derives from this result, the equality of momentum and mass transport allows the extension of experimentally-measured quantities. For example, a measurement of liquid volume fraction provides an estimate of the local velocity.

The derivation assumed that the injection velocity was constant. This is a restrictive assumption that could potentially be relaxed. Musculus [3] applied the method of characteristics to the study of transient jets. Perhaps application of a similar method could allow this result to be generalized to transient sprays.

[1] No relation to the first author

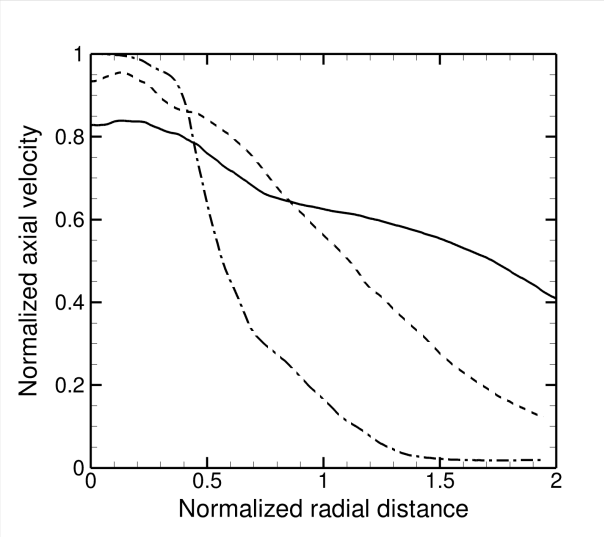

Figure 7. Tangentially-averaged axial velocity profiles obtained by time averages of the CFD simulation at three distinct locations, located at 7.8 (dash-dot line), 19 (dashed line), and 52 (continuous line) orifice diameters d_0 from the nozzle exit. The radial distance is normalized by d_0 and the velocity is normalized by the maximum axial value u_{MAX}.

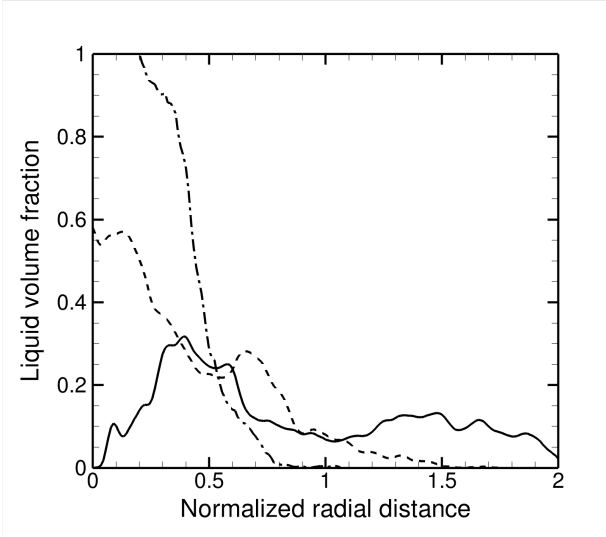

Figure 8. Tangentially-averaged liquid volume fraction profiles obtained by time averages of the CFD simulation at three distinct locations, located at 7.8 (dash-dot line), 19 (dashed line), and 52 (continuous line) orifice diameters d_0 from the nozzle exit. The radial distance is normalized by d_0.

In particular, the derivation of Eqn. 22 assumed that the denominator of the definition of L^* is constant. However, one could potentially follow the equation characteristics at a speed of $\beta\bar{u}$ emanating from the orifice in a transient injection and extend this analysis to transient injections. If such a generalization is possible, then this line of analysis could lead to a new branch of spray modeling approaches.

The analysis and comparison with high-fidelity results also raised some questions. How can the apparent contradiction in the mathematics be resolved? The analysis assumes that the velocity profile and LVF profile are similar, but the results show a similarity instead between the momentum profile and LVF profile. This discrepancy is likely due to the simplification that Musculus and Kattke made in their momentum flux.

The comparison to high fidelity spray simulation results begin to address the question of what similarities are found in actual sprays. Given the high density ratio between phases, is it reasonable to expect that the unity Schmidt number assumption holds? Certainly, the transport of liquid mass into a region consisting of primarily of gas represents a shift of the center of mass that would not be observed in a uniform density gas jet. This difference between sprays and jets is significant because gas jets often serve as an inspiration for mixing-limited spray analyses.

Acknowledgments

Support by the Spray Combustion Consortium of automotive industry sponsors, including Convergent Science Inc., Cummins Inc., Ford Motor Co., Hino Motors Ltd., Isuzu Motors Ltd., Groupe Renault, and Toyota Motor Co., is gratefully acknowledged.

Sandia National Laboratories is a multi-mission laboratory managed and operated by National Technology and Engineering Solutions for Sandia LLC, a wholly owned subsidiary of Honeywell International, Inc., for the U.S. Department of Energy's National Nuclear Security Administration under contract DE-NA0003525.

References

[1] Mark PB Musculus and Kyle Kattke. *SAE International Journal of Engines*, 2(1):1170–1193, 2009.

[2] Dennis L Siebers. Scaling liquid-phase fuel penetration in diesel sprays based on mixing-limited vaporization. Technical report, SAE technical paper, 1999.

[3] Mark PB Musculus. *Journal of Fluid Mechanics*, 638:117–140, 2009.

[4] Lyle M Pickett, Julien Manin, Caroline L Genzale, Dennis L Siebers, Mark PB Musculus, and Cherian A Idicheria. *SAE International Journal of Engines*, 4(1):764–799, 2011.

[5] Sanghoon Kook and Lyle M Pickett. *Fuel*, 93:539–548, 2012.

[6] Michele Bardi, Raul Payri, Louis Marie C Malbec, Gilles Bruneaux, Lyle M Pickett, Julien Manin, Tim Bazyn, and Caroline L Genzale. *Atomization and Sprays*, 22(10), 2012.

[7] Alan L Kastengren, Christopher F Powell, Seong-Kyun Cheong, Yujie Wang, Kyoung-Su Im, Xin Liu, Jin Wang, and Thomas Riedel. Determination of diesel spray axial velocity using x-ray radiography. Technical report, SAE Technical Paper, 2007.

[8] Marco Arienti and Mark Sussman. *International Journal of Multiphase Flow*, 88:205–221, 2017.

[9] Michele Battistoni, Gina M Magnotti, Caroline L Genzale, Marco Arienti, Katarzyna E Matusik, Daniel J Duke, Jhoan Giraldo, Jan Ilavsky, Alan L Kastengren, Christopher F Powell, et al. *SAE International Journal of Fuels and Lubricants*, 11(4):337–352, 2018.

[10] Matthew Jemison, Mark Sussman, and Marco Arienti. *Journal of Computational Physics*, 279:182–217, 2014.

[11] R Payri, JM García, FJ Salvador, and Jaime Gimeno. *Fuel*, 84(5):551–561, 2005.